Theoretical Chemistry Accounts (2020) 139:167
https://doi.org/10.1007/s00214-020-02680-2

REGULAR ARTICLE

On the hydrogen storage performance of Cu-doped and Cu-decorated graphene quantum dots: a computational study

Michal Malček[1] · **Lukáš Bučinský**[1]

Received: 4 March 2020 / Accepted: 5 October 2020 / Published online: 22 October 2020

Abstract
Hydrogen gas is a promising renewable energy source. The hydrogen storage performance of two differently modified graphene surfaces, particularly Cu-doped and Cu-decorated circumcoronene (CC), is investigated using density functional theory, 6-311G* basis set and Bader's quantum theory of atoms in molecules (QTAIM). It is found that the Cu-doped CC is able to bind three H_2 molecules on one Cu atom, while the Cu-decorated CC is able to bind up to five H_2 molecules on one Cu atom. Changes in the topology of charge density upon the H_2 adsorption are evaluated under the formalism of QTAIM analysis. The QTAIM analysis of bond critical points as well as the density of states analysis show that the interaction between Cu and adsorbed H_2 molecules can be considered as a physisorption (a van der Waals type interaction). Overall, the results presented in this study point out that the Cu-decorated graphene surfaces are more suitable potential candidates for hydrogen storage than the Cu-doped ones. Furthermore, the inclusion of diffuse functions in the basis set is critically considered.

Keywords Circumcoronene · DFT · Graphene quantum dots · Electronic structure · Hydrogen storage · QTAIM analysis

1 Introduction

In the last two decades, graphene based materials have attracted a huge attention due to their extraordinary chemical, mechanical, electronic and optical properties [1–7]. Graphene, rediscovered and isolated in 2004 [1], is a two dimensional monolayer of sp^2-hybridized carbon atoms arranged in a hexagonal honeycomb lattice. In 2007, Schedin et al. [3] have proposed an idea to use graphene materials as adsorbents of individual gas molecules. However, the pristine graphene behaves like a zero-band-gap semiconductor, due to the overlap of its valence and conduction bands at the Brillouin zone [8]. Opening of this band gap is highly desirable because it significantly enhances the electronic properties and chemical reactivity of graphene materials [8]. Opening of this bang gap can be performed either by doping (i.e. replacing a carbon atom with the dopant atom) or by decorating (i.e. placing a heteroatom above the carbon layer) of the graphene surfaces (GS) with different heteroatoms [9–18]. Among many transition metals, copper and its oxides have been used as possible dopants or decorating atoms of GS in both theoretical and experimental studies [9, 10, 13, 14, 19–21]. For example, in the theoretical work of Düzenli [10], the Cu-doped GS has been reported as the most efficient H_2O_2 adsorbent. Mohammadi-Manesh et al. [13, 14] have studied the adsorption of H_2S on the GS decorated with Cu, CuO and Cu_2O using density functional theory (DFT), particularly PBE functional. Very recently, a suitability of Cu-doped and Cu-decorated GSs as powerful adsorbents has been demonstrated for a series of organic molecules employing QTAIM analysis [20, 22]. From the synthetic point of view, several experimental attempts to prepare graphene materials decorated with copper atoms [23–25], or covered with Cu^{2+} cations [26] have been reported. Still, it has to be mentioned that the synthesis of Cu–GS units with well define dimension depends strongly on the reaction time, concentration, voltage, electric current and other conditions [23–25, 27].

Published as part of the topical collection of articles from the 17th edition of the Central European Symposium on Theoretical Chemistry (CESTC 2019) in Austria

Electronic supplementary material The online version of this article (https://doi.org/10.1007/s00214-020-02680-2) contains supplementary material, which is available to authorized users.

✉ Michal Malček
michal.malcek@stuba.sk

[1] Faculty of Chemical and Food Technology, Institute of Physical Chemistry and Chemical Physics, Slovak University of Technology in Bratislava, Radlinského 9, 812 37 Bratislava, Slovak Republic

Hydrogen gas is a promising clean and renewable energy source [28]. However, it is difficult to store the hydrogen gas (H_2) under ambient conditions due to weak interactions among the H_2 molecules. The first crucial step in the storage process of the particular gas (in this case H_2) is its efficient adsorption on the adsorbent material. It has been shown that the hydrogen molecule exhibits only weak affinity towards the pristine graphene surface [29]. Nevertheless, a number of theoretical studies of hydrogen storage performance of different doped graphene surfaces are rapidly increasing [29–35]. For example, the hydrogen storage ability of Cr-doped graphene nanoflakes (GS) has been theoretically studied by Xiang et al. [29]. Xiang et al. [29] have reported that three H_2 molecules can be adsorbed on each Cr atom. Similarly, Zhou et al. [31] have reported that three H_2 molecules can be stored on one Li atom of Li-doped GS. Tabtimsai et al. [30] have studied the H_2 adsorption on GS doped with different transition metals. The strongest binding ability towards H_2 has been reported for Os-doped GS, being able to store three H_2 molecules on one Os atom [30]. Faye and coworkers [34] have shown that the presence of boron dopant within the Cu-functionalized (decorated) GS enhances the H_2 adsorption. Still, the reported maximum number of adsorbed H_2 molecules on one Cu atom is three [34]. With respect to what is mention above, one can conclude that the storage ability of doped GS is three H_2 molecules on one transition metal [29–31]. The interaction of Cu atom with the H_2 molecule has been also intensively studied in the past [36].

In the presented paper, the hydrogen storage performance of copper-doped and copper-decorated circumcoronene is studied combining the methods of density functional theory (DFT) and Bader's quantum theory of atoms in molecules (QTAIM) [37]. A comparison between the suitability of these two differently modified GSs as hydrogen adsorbents is discussed as well. The results of this work are presented in Sect. 3 which is subdivided into three main parts. The first subsection is focused on the structural parameters, i.e. bond distances and their changes upon the H_2 adsorption. In the second subsection, calculated adsorption energies and LUMO–HOMO band gaps are considered including the assessment of orbital positioning obtained from the PDOS analysis. QTAIM charge density topology and analysis of bond critical points (BCP) and delocalization indexes (DI) are discussed in the third subsection.

2 Computational details

Circumcoronene (CC) is a polyaromatic hydrocarbon composed of 54 carbon atoms arranged in 19 hexagonal rings. It has been previously used as a model system of the graphene quantum dot (GQD), [20, 22, 29, 30, 38–41] because it has a high symmetry and sufficient yet reasonable size from the computational point of view. Optimized geometries (B3LYP/6-311G* level of theory) of Cu-doped and Cu-decorated CC were taken from authors' previous works, [20, 22] considering only the most stable positions of dopant or decorating Cu atom. These geometries were re-optimized using the B3LYP [42–45] functional including the D3 version of Grimme's dispersion correction (GD3) [46] and the same basis set as mentioned above [47–49]. The inclusion of GD3 correction is essential for a proper treatment of adsorption energies and geometries, because standard DFT normally fails in a description of the long-range van der Waals interactions [50–52]. Even though the GD3 correction may overestimate the interaction energies [53], it is still a very good choice when taking into account its accuracy and computational cost [54]. From hereafter, the Cu-doped and Cu-decorated CC will be abbreviated as "Cu-dopCC" and "Cu-decCC", respectively. Structure of the optimized Cu-doped and Cu-decorated CC (including both side- and top-view) is shown in Fig. 1

Hydrogen molecules (H_2) were placed in the vicinity of the Cu atom in both studied systems with the initial distance between the H_2 and Cu being from interval of 2.2–2.5 Å. Number of interacting H_2 molecules was varied from one to five for both systems under study. Subsequent geometry optimizations were performed at the same level of theory, i.e. B3LYP-GD3 [42–46]/6-311G* [47–49]. The energy-based criterion of the SCF convergence was set to 10^{-8} Hartree in all calculations. All systems containing Cu were treated as doublets using the unrestricted Kohn–Sham formalism. Vibrational analysis was employed to confirm that the optimal geometries correspond to energy minima (i.e. no imaginary vibrations). All the aforementioned DFT calculations were carried out using the Gaussian09 program package [55]. QTAIM analysis [37] as implemented in the AIMAll package [56] was performed for every system under study using the Gaussian09 checkpoint files. This analysis was employed to evaluate charge and spin densities at the particular atoms (especially Cu) as well as to estimate the character of interatomic (or intermolecular) interactions via analysis of bond critical points (BCP) and delocalization indexes (DI). Density of states (DOS) and partial density of states (PDOS) calculations were carried out using the GaussSum package [57] to get insight into the molecular orbitals overlapping. Visualization of the optimized structures was performed using the Molekel software suite [58].

To check the results consistency with respect to the basis set used, additional geometry optimizations of the systems with one adsorbed hydrogen molecule (i.e. Cu-dopCC + H_2 and Cu-decCC + H_2) were performed using 6-311G**, 6–311++G* and 6–311++G** [47–49, 59] basis sets.

The basis set superposition error (BSSE) corrected E_{ads}^{BSSE} adsorption energies between the Cu-dopCC or Cu-decCC

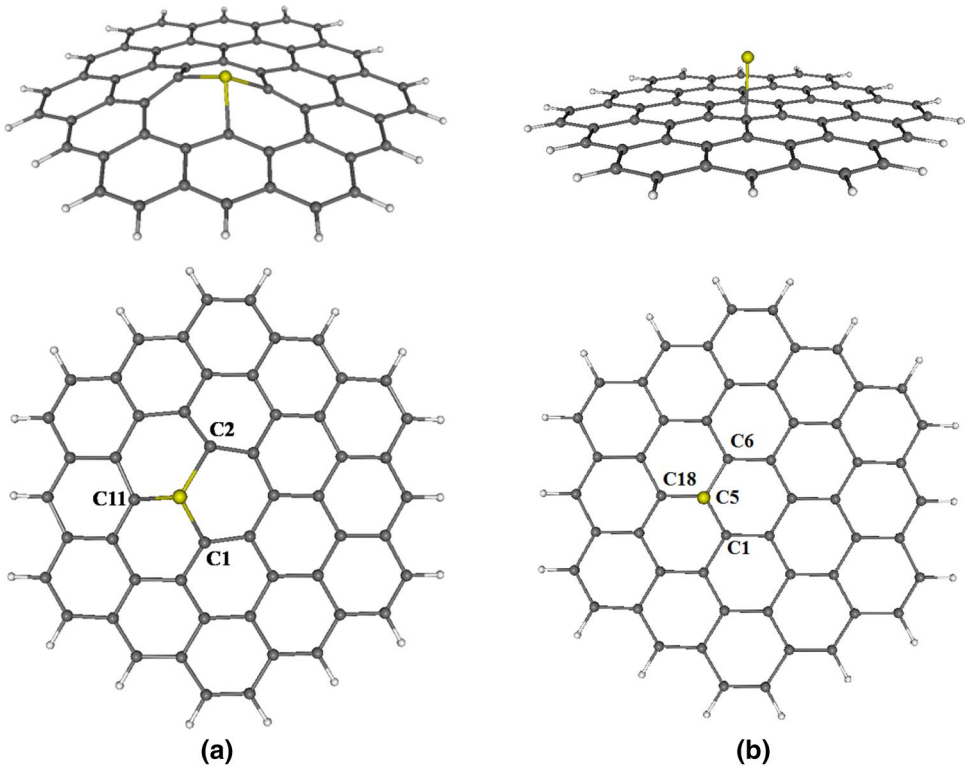

Fig. 1 Scheme of the B3LYP-GD3/6-311G* optimized Cu-doped (**a**) and Cu-decorated (**b**) CC including relevant atom labelling (note that in the case of Cu-decorated CC is carbon C5 directly under Cu atom)

systems and the H_2 molecules were calculated using the equation

$$E_{\text{ads}}^{\text{BSSE}} = E_{\text{CuCC}/nH2} - (E_{\text{CuCC}}^{\text{BSSE}} + E_{\text{nH2}}^{\text{BSSE}}) \quad (1)$$

where $E_{\text{CuCC/nH2}}$ is the energy of system with n adsorbed hydrogen molecules, $E_{\text{CuCC}}^{\text{BSSE}}$ and $E_{\text{nH2}}^{\text{BSSE}}$ are the BSSE corrected energies of Cu-dopCC or Cu-decCC and n H_2 molecules, respectively, calculated via the counterpoise scheme of Boys and Bernardi [60]. Number of H_2 molecules ranges from one to five. It has to be noted that in some of the counterpoise scheme calculations for evaluating the BSSE corrected energies a quadratically convergent (QC) SCF procedure [61] had to be employed because of their problematic convergence.

3 Results and discussion

3.1 Structural parameters

The calculated distances between the Cu and the hydrogens from adsorbed H_2 molecules as well as between the Cu and the neighbouring or adjacent carbons of CC backbone for all studied systems are compiled in Table 1. Doping the CC backbone with Cu leads to the perturbation of its originally planar structure due to the larger number of electron shells of Cu when compared to carbon [10, 20], see Fig. 1a. On the other hand, decorating of the CC backbone with Cu preserves its planar (honeycomb) structure [13, 14, 22], see Fig. 1b. In this study, a distance between the Cu atom and CC backbone in Cu-decCC optimized at the B3LYP-GD3/6-311G* level of theory is 2.07 Å (see Cu–C5 value in Table 1). For comparison, the B3LYP/6-311G* Cu–C5 distance reported in one of our previous studies is 2.06 Å [22]. Mohammadi-Manesh et al. have reported the Cu-GS distance of 2.12 Å using the PBE functional with pseudopotentials [13]. Naturally, a Cu atom as an (H_2) acceptor site is sterically significantly less hindered in the Cu-decCC than in the case of Cu-dopCC as can be seen in Fig. 1.

As can be seen from Table 1, the Cu-dopCC is able to adsorb (or store) three H_2 molecules, the fourth one is too distant from the Cu acceptor site (see Cu–H distance of 3.65 Å in Table 1). This is further confirmed by the presence of only three Cu–H bond critical points found in Cu-dopCC + $4H_2$ system, see the section QTAIM charge density topology and bond critical points analysis. The obtained number of adsorbed H_2 molecules corresponds well with the previously published results [29–31, 34] where fourth and/or fifth H_2 molecule are found to be significantly more distant from the dopant atom (Cr, Li, Os, Cu, etc.) than the other three ones. Hence, we can confirm that the ability to store three H_2 molecules seems to be the limit of the doped CC (or doped GS in general). All of the adsorbed H_2 molecules (one, two or three) on the Cu-dopCC are found within the distance of 2.5–2.7 Å from Cu atom. On the other hand, in the case

Table 1 Optimized B3LYP-GD3/6-311G* Cu–H and Cu–C distances in Cu-dopCC and Cu-decCC

System	Distances/Å				
	Cu–H	Cu–C1	Cu–C2	Cu–C11	
Cu-dopCC		1.84	1.86	1.86	
$+H_2$	2.65	1.84	1.87	1.87	
$+H_2$ $^{6-311G**}$	2.62	1.84	1.87	1.87	
$+H_2$ $^{6-311++G*}$	1.75	2.24	1.96	2.34	
$+H_2$ $^{6-311++G**}$	1.71	2.25	1.96	2.35	
$+2H_2$	2.52, 2.61	1.86	1.88	1.88	
$+3H_2$	2.49, 2.57, 2.55	1.87	1.89	1.89	
	Cu–H	Cu–C5	Cu–C6	Cu–C1	Cu–C18
Cu-decCC		2.07	2.60	2.60	2.62
$+H_2$	2.64	2.09	2.61	2.62	2.64
$+H_2$ $^{6-311G**}$	2.63	2.09	2.61	2.61	2.64
$+H_2$ $^{6-311++G*}$	2.76	3.08	3.55	3.11	3.50
$+H_2$ $^{6-311++G**}$	2.76	3.08	3.50	3.55	3.11
$+2H_2$	2.64, 2.64	2.09	2.59	2.63	2.65
$+3H_2$	2.61, 2.62, 2.61	2.10	2.63	2.62	2.63
$+4H_2$	2.62, 2.60, 2.60, 2.61	2.11	2.66	2.59	2.65
$+5H_2$	2.64, 2.66, 2.66, 2.68, 2.68	2.15	2.68	2.66	2.68

For C atoms labelling see Fig. 1. For comparison, the optimized Cu–H and Cu–C distances obtained by using different basis sets are presented for the systems with one adsorbed H_2 molecule

of Cu-decCC up to five H_2 molecules can be adsorbed on the Cu atom: all five Cu–H distances in the Cu-decCC + $5H_2$ system are from the interval of 2.64–2.68 Å, see Table 1. This higher H_2 adsorption capacity of Cu-decCC (five) when compared to Cu-dopCC (three) can be mainly assigned to the steric constraints in Cu-dopCC. Naturally, the adsorption of H_2 molecules leads to a small destabilization of the Cu atom upon the CC surface, what is reflected in the increase of Cu–C5 (in Cu-decCC) and Cu–C1, Cu–C2 and Cu–C11 (in Cu-dopCC) bond lengths, see Table 1. These small changes in Cu–C bonds will be further discussed in the section QTAIM charge density topology and bond critical points analysis. For completeness, schematic drawings of Cu-dopCC and Cu-decCC systems with the adsorbed H_2 molecules optimized at the B3LYP-GD3/6-311G* level of theory are shown in Figs. 2 and 3, respectively. Side-views of all the studied systems are provided in Figs. S1 and S2 in electronic supporting information (ESI). The H–H bond lengths in all adsorbed H_2 molecules are around 0.74 Å what corresponds to the H–H bond in the molecular hydrogen.

Last but not least, an effect of the different basis sets used (different than 6-311G*) has to be discussed. The inclusion of diffuse functions into the basis set (i.e. employing 6–311++G* and 6–311++G** basis sets) leads to a considerable change in the interactions between the Cu atom and the CC backbone. In the case of the Cu-dopCC system, perturbations in the CC backbone occur which are similar as found for the Cu-doped surfaces reported in one of our previous works [20]. In addition, the Cu atom in the 6–311++G** optimized Cu-dopCC binds the H_2 molecule in a side-on way (as illustrated in Fig. S3), while when using 6-311G* basis set, the Cu–H_2 interaction has an end-on nature (see Fig. S1). Interestingly, as reported by Ruíz and coworkers [36], the side-on attack of the Cu atom on the H_2 molecule is typical for the ^2P excited state of Cu. (The Cu electronic states ^2S, ^2D, ^2P correspond to the valence electron configurations $3d^{10}4s^1$, $3d^94s^2$, $3d^{10}4p^1$, respectively [36, 62].) In the case of the Cu-decCC system, the Cu–CC distance becomes destabilized by almost one Å and the H_2 molecule becomes adsorbed above the CC backbone. The diffuse functions within the 6–311++G** basis set are crucial for the assessment of the ^2S ground state of Cu, while for the 6-311G* basis set an admixture of ^2S and ^2D states is identified as the ground state.

3.2 Adsorption energies, LUMO–HOMO band gaps and density of states analysis

The calculated BSSE corrected adsorption energies (E_{ads}^{BSSE}) and α and β LUMO–HOMO band gaps ($E_{LUMO-HOMO}$) of all studied systems are compiled in Table 2. The importance of BSSE correction in the calculations of adsorption energies has been already discussed in our previous work [22]. As can be seen from Table 2, the calculated adsorption energies are naturally getting higher with increasing number of adsorbed H_2 molecules. In the case

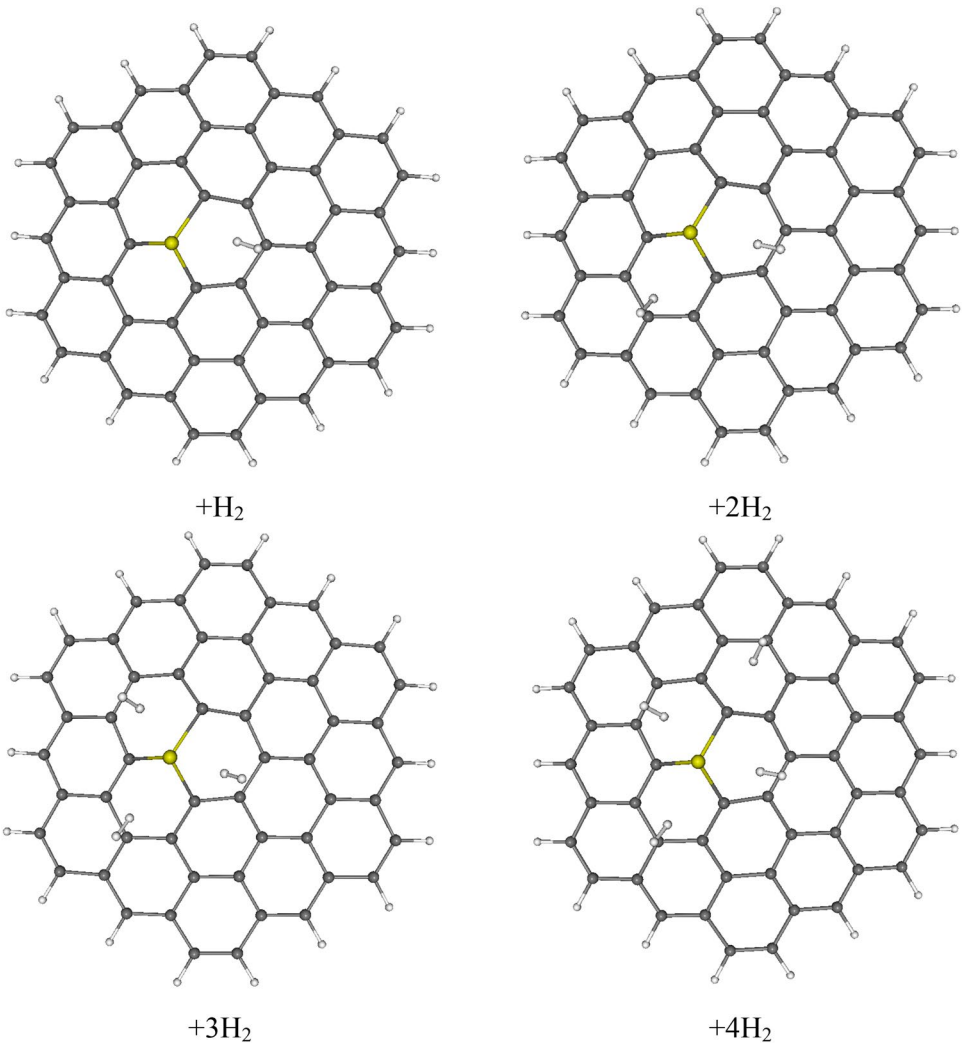

Fig. 2 Scheme of the optimized B3LYP-GD3/6-311G* Cu-dopCC plus interacting H_2 molecules

of Cu-dopCC system is this increase approximately linear ranging from −6.7 up to −24.8 kJ mol^{-1}, i.e. around 6 kJ mol^{-1} with every H_2 molecule adsorbed, see Table 2. On the other hand, in the case of Cu-decCC system is the increase of E_{ads}^{BSSE} values rather exponential with respect to the number of adsorbed H_2 molecules, ranging from −0.3 up to −30.5 kJ mol^{-1} (see Table 2). It has to be mentioned that the B3LYP functional (without GD3 long range correction) fails in calculating adsorption energies, as is written above in Computational details section. The use of B3LYP functional does not provide negative adsorption energies but positive ones. It is also worth to point out that the adsorption energies of hydrogens on Cu atom are an order of magnitude lower than the ones of oxygen, water or methanol reported in our previous studies [20, 22]. This large difference is due to the higher affinity of Cu towards the O atom (e.g. in O_2) [63] than towards the H atom.

Both alpha and beta LUMO–HOMO band gaps ($E_{LUMO–HOMO}$) as well as spin squared expectation values (S^2) of the studied systems are also presented in Table 2. Alpha partial density of states (PDOS) of Cu and H atoms in Cu-dopCC and Cu-decCC systems (including the identification of LUMO–HOMO gap) are shown in Figs. 4 and 5, respectively. The $E_{LUMO–HOMO}$ values of all the systems under study are only negligibly affected by the adsorbed H_2 molecules, as can be seen from Table 2 and Figs. 4 and 5. The differences in $E_{LUMO–HOMO}$ values are less than 0.1 eV (Table 2) because there are only negligible changes in the *d* and *s* valence shells of Cu near Fermi level upon the H_2 molecules adsorption (see the red lines in Figs. 4 and 5 at ca. −4 eV). Nevertheless, all of the LUMO–HOMO band gaps reported here are significantly lower than the band gap in the pristine CC (being around 2.8 eV) [22] due to the doping or decorating with transition metal (in this case Cu) [8, 9]. The larger β LUMO–HOMO band gap (ca. 2.7 eV) in comparison to the α one (ca. 1.3 eV) in Cu-decCC is caused by the presence of one unpaired α 4 *s* electron of Cu, represented by the small red dashed peak at ca. −3 eV

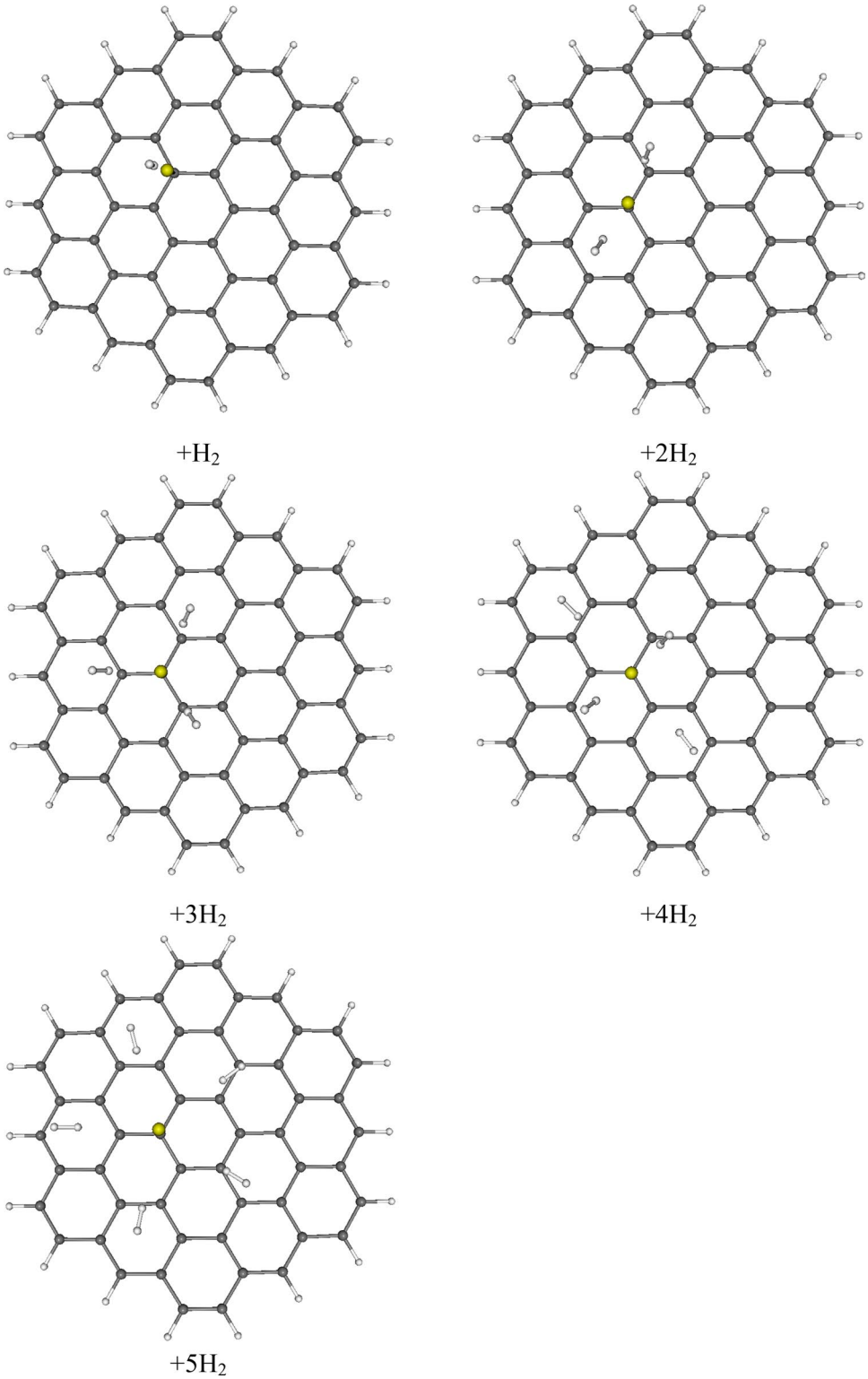

Fig. 3 Scheme of the B3LYP-GD3/6-311G* optimized Cu-decCC plus interacting H_2 molecules

in Fig. 5. The values of spin contamination presented in Table 2 correspond to the theoretical value of 0.75 for a single unpaired electron.

As can be seen from the PDOS analysis of Cu-dopCC + *n* H_2, there is only a small overlap between the *s* or *d* electrons of Cu (red dashed or red solid lines, respectively) and the valence electrons of adsorbed H_2 molecules (blue, cyan and green lines) at ca. 2 eV and ca. −12 eV, see Fig. 4. Even smaller or almost negligible overlap between the valence electrons of Cu and H_2 molecules is found in PDOS plots

Table 2 B3LYP-GD3/6-311G* BSSE corrected (E_{ads}^{BSSE}) adsorption energies, LUMO–HOMO band gap energies ($E_{LUMO-HOMO}$) in eV and spin contamination (S^2) of all studied systems. The superscripts α and β stand for alpha and beta LUMO–HOMO band gaps, respectively

System	E_{ads}^{BSSE}/kJ mol^{-1}	$E_{LUMO-HOMO}$/eV	S^2
Cu-dopCC		1.89^{α}, 1.65^{β}	0.777
$+H_2$	−6.73	1.85^{α}, 1.66^{β}	0.778
$+2H_2$	−13.48	1.89^{α}, 1.66^{β}	0.778
$+3H_2$	−18.14	1.92^{α}, 1.69^{β}	0.773
$+4H_2$	−24.75	1.91^{α}, 1.69^{β}	0.773
Cu-decCC		1.41^{α}, 2.67^{β}	0.753
$+H_2$	−0.36	1.35^{α}, 2.70^{β}	0.752
$+2H_2$	−3.49	1.30^{α}, 2.71^{β}	0.753
$+3H_2$	−7.41	1.26^{α}, 2.72^{β}	0.753
$+4H_2$	−15.80	1.24^{α}, 2.72^{β}	0.754
$+5H_2$	−30.54	1.32^{α}, 2.71^{β}	0.753

of Cu–decCC + n H_2, see small peaks at ca. 2 eV in Fig. 5. These results hand-in-hand with the relatively long Cu–H distances (Table 1) and small changes in LUMO–HOMO gaps (Table 2) point out that the interaction of Cu with H_2 molecules in the studied systems is driven rather by "physical" van der Waals forces than the "chemical" (electronic) ones. The character of these Cu–H interactions will be discussed in more detail via analysis of bond critical points in the coming section.

For completeness, the calculated B3LYP-GD3/6-311G* harmonic frequencies, representing the IR spectra, of the studied systems are presented in Figs. S4 and S5. As illustrated in Fig. S4, the Cu–CC, C–H and H–H vibrations are found in the regions of ca. 1250, 3200 and 4200 cm^{-1}, respectively. For comparison, a calculated B3LYP-GD3/6-311G* energy of H–H vibration in a single hydrogen molecule is 4393 cm^{-1}. Interestingly, an adsorption of H_2 molecules on the Cu-dopCC system has no effect on the

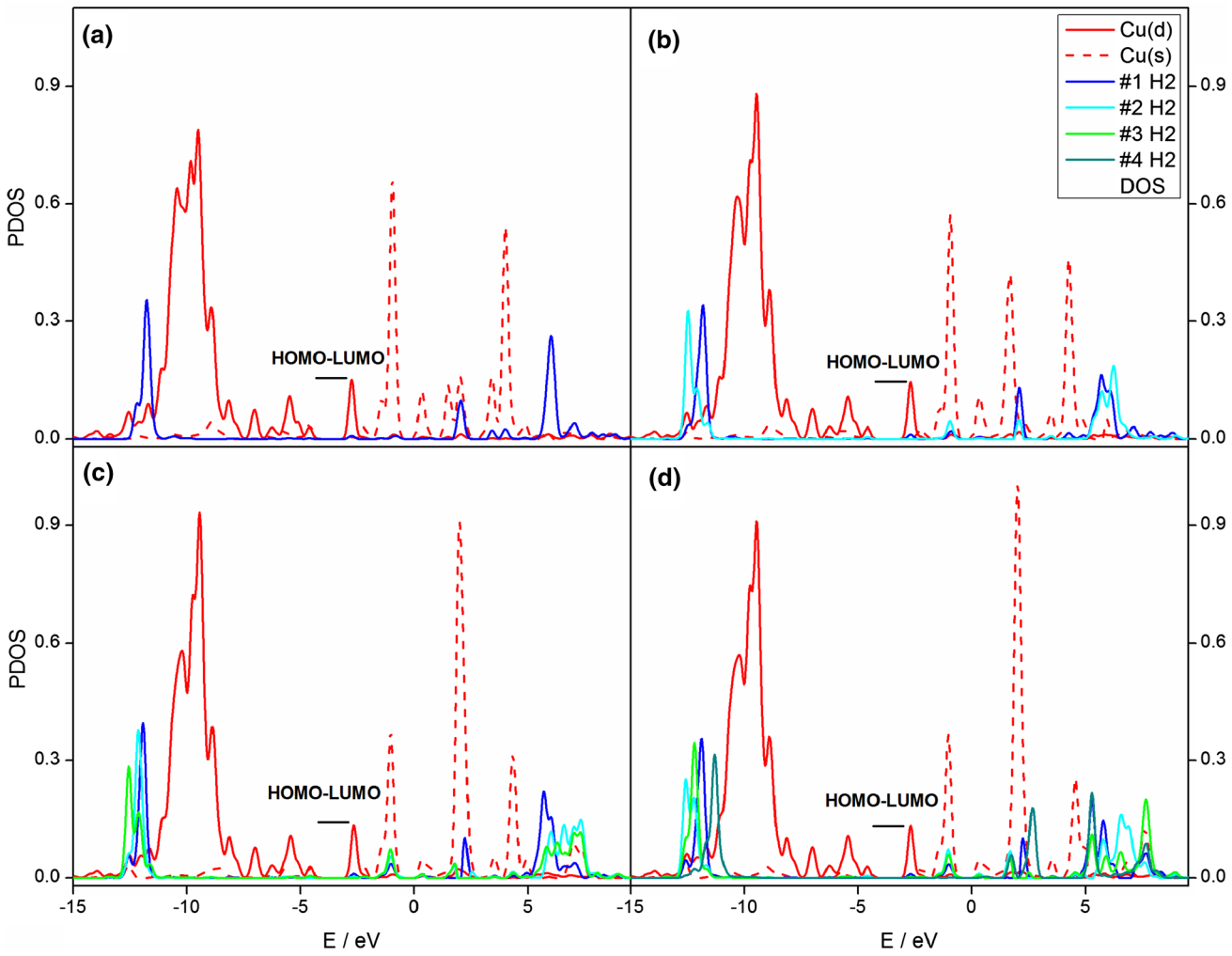

Fig. 4 α PDOS of Cu–H bond in Cu-dopCC + H_2 (**a**), + 2 H_2 (**b**), + 3 H_2 (**c**), + 4 H_2 (**d**). The particular α LUMO–HOMO band gaps are depicted as well. All plots are obtained at the B3LYP-GD3 level of theory and for comparison purposes the absolute scale is used

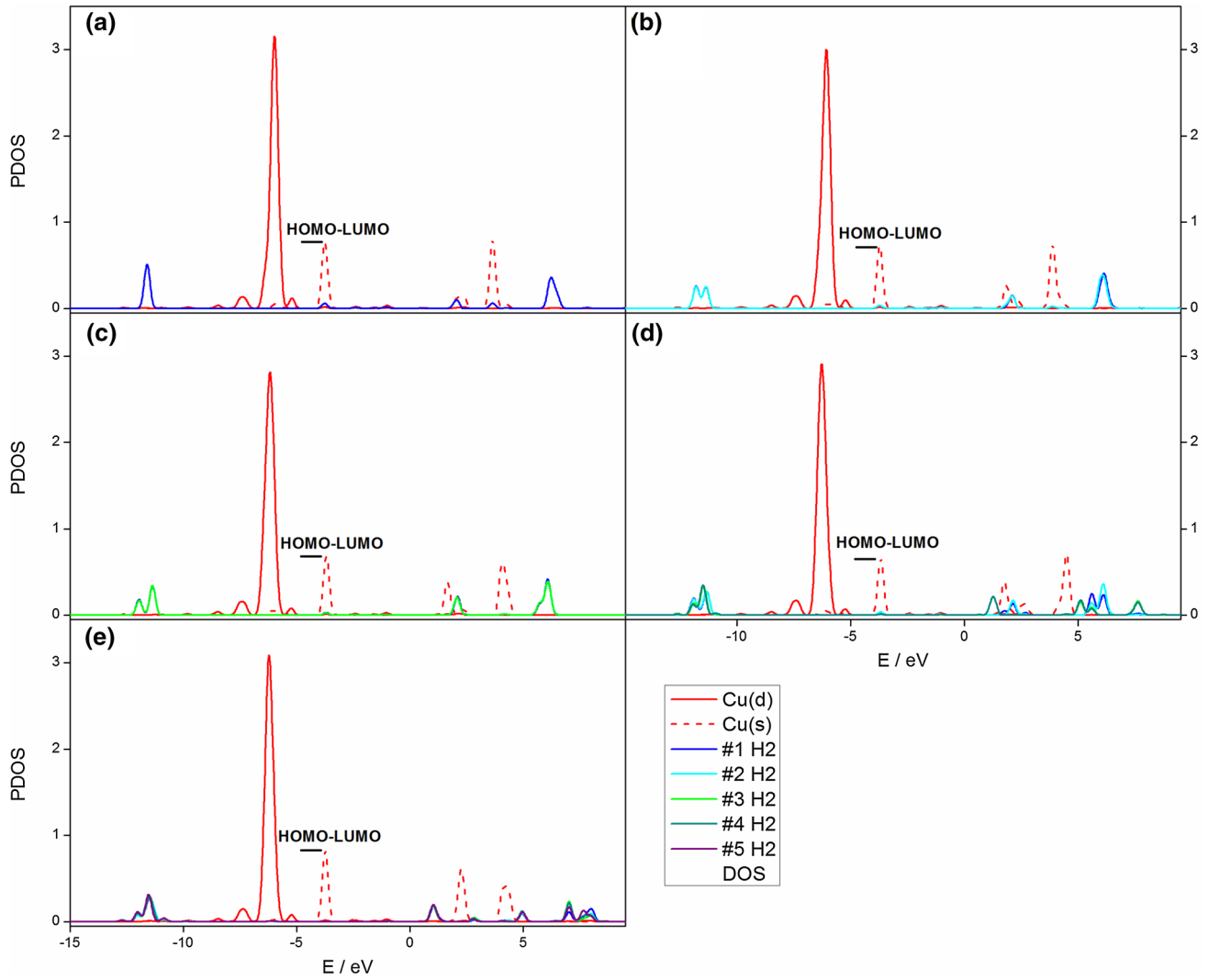

Fig. 5 α PDOS of Cu–H bond in Cu-decCC + H_2 (**a**), + 2 H_2 (**b**), + 3 H_2 (**c**), + 4 H_2 (**d**), + 5 H_2 (**e**). The particular α LUMO–HOMO band gaps are depicted as well. All plots are obtained at the B3LYP-GD3 level of theory and for comparison purposes the absolute scale is used

calculated Cu–CC vibrations, while in the case of Cu-decCC system, the interaction with H_2 leads to the decrease in IR intensities of these vibrations (Cu–CC), see Fig. S5. Hence, an adsorption of H_2 molecules on the Cu-decorated graphene materials should be experimentally detected in the IR spectra.

3.3 QTAIM charge density topology and bond critical points analysis

Bader's quantum theory of atoms in molecules (QTAIM) [37] presents a useful tool to analyse the charge and/or spin density distribution using the gradient vector field of the electron density, $\nabla\rho(r)$. The effective atomic charges and spin densities are established upon the formal decomposition of a particular molecule into atomic domains, so-called basins. The QTAIM charge and spin densities at Cu as a function of the number of adsorbed H_2 molecules in Cu-dopCC and Cu-decCC are shown in Fig. 6. For completeness, the partial QTAIM charges (or spins) at Cu and hydrogen molecules of all studied systems are compiled in Table S1 in ESI. In the case of Cu-dopCC there is only a negligible charge transfer from the adsorbed H_2 molecules: partial charge and spin densities at Cu are around 0.67 and 0.18 e, respectively, (Fig. 6, left) while adsorbed hydrogens have only slightly negative charges (up to −0.019 e see Table S1) which can be considered negligible. For completeness, spin density distribution maps of the Cu-dopCC systems are provided in Fig. S6 in ESI. On the other hand, in the case of Cu-decCC, the positive charge of Cu atom increases with every adsorbed H_2 molecule (see Fig. 6, right) ranging from ca. 0.15 up to ca. 0.30 e. Correspondingly, the spin density of Cu atom

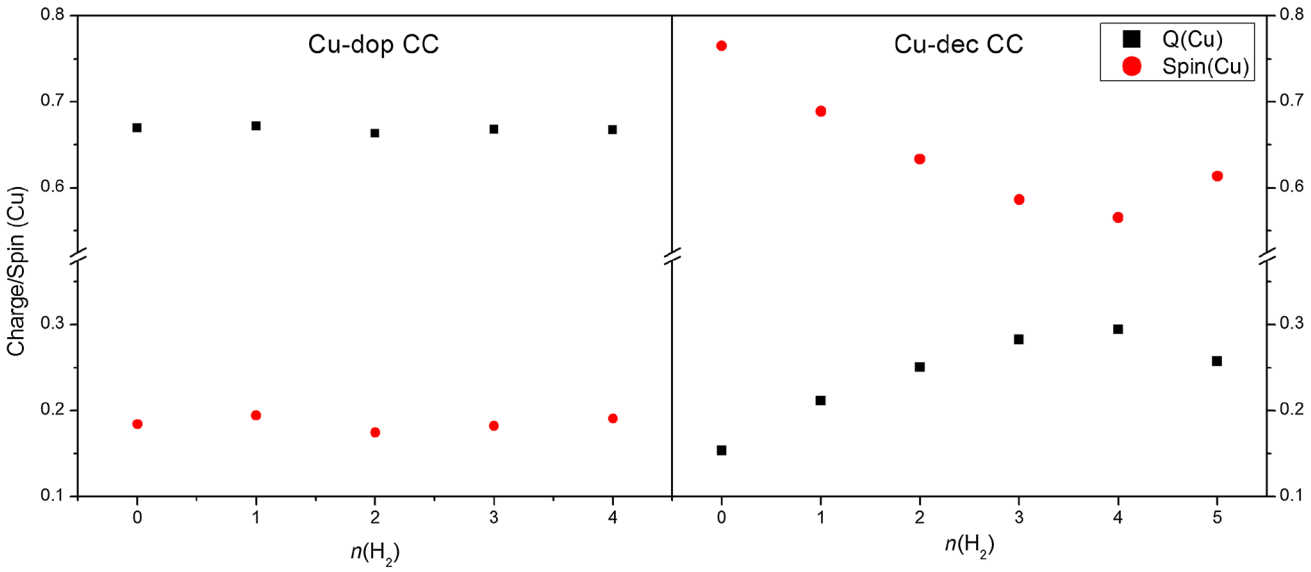

Fig. 6 QTAIM charge and spin densities at Cu in Cu-dopCC (left) and Cu-decCC (right) as a function of number of adsorbed H_2 molecules [$n(H_2)$]

decreases upon the adsorption of H_2 molecules (see Fig. 6, right). Spin density distribution maps of the Cu-decCC systems are provided in Fig. S7 in ESI. This charge transfer is reflected in the increased negative charges of adsorbed H_2 molecules (ranging from −0.035 to −0.072 e, see Table S1) as well as in their spin densities (ranging from 0.037 to 0.096 e, see Table S1). From these values, one can clearly see that it is the unpaired electron density which is partially transferred from the Cu atom to the adsorbed H_2 molecules (cf. Figure 6 and Table S1). Interestingly the Cu charge (or spin) dependence of the number of adsorbed H_2 molecules is not divergent, but it has a local maximum (or minimum) in the case of Cu-decCC + 4 H_2 system.

The character (or nature) of chemical bonds can be further inspected using the QTAIM analysis of bond critical points (BCPs). The BCP is a saddle point of electron density between two atoms forming a chemical bond [37]. Strength of the chemical bond can be estimated from the charge density in the BCP (ρ_{BCP}). Laplacian of charge density in BCP ($\Delta\rho_{BCP}$) can be either negative or positive depending on whether electronic charge is locally concentrated or depleted [37]. Ellipticity of the electron density (ε_{BCP}) is, in general, associated with π character of chemical bonds, hence it can be used as a measure of aromaticity [64]. Delocalization index (DI) is another useful parameter, being a measure of the number of electrons that are shared between two atoms [65]. The BCP electron densities, their Laplacians and DIs of the formed Cu–H bonds in all studied systems are presented in Figs. S8, S9 and 7, respectively. For completeness, the particular values of the BCP characteristics and DIs are given in Table S2 in ESI. Interestingly, the Cu–H bonds of Cu-dopCC + n H_2 systems are getting stronger with every adsorbed H_2 molecule (up to three H_2 molecules) as can be seen from Figs. S8, S9 and 7. However, the particular Cu–H ρ_{BCP} and DI values are still very small, i.e. ca. 0.01 bohr^{-3} and 0.04–0.05, respectively. The situation is similar also in the case of Cu-decCC + n H_2 systems: only weak Cu–H bond interaction with ρ_{BCP} of ca. 0.01 bohr^{-3}. On the other hand, the DI values of Cu–H bonds in Cu-decCC + n H_2 have the opposite trend than the ones of Cu-dopCC + n H_2, as can be seen in Fig. 7. In this case, the strongest Cu–H bond is found in Cu-decCC + H_2 having the DI value of 0.124, even though ρ_{BCP} is still only 0.01 bohr^{-3} (see Fig. 7 and Table S2). For comparison, Afonin et al. [66] have reported that the moderate hydrogen bond between H and O has ρ_{BCP} of ca. 0.04 bohr^{-3} what is four-times larger than our calculated values. This is in agreement with the results presented in the Adsorption energies, LUMO–HOMO band gaps and Density of States analysis section, showing that the interaction between Cu and hydrogens is of van der Waals type.

Another parameter to be monitored upon the adsorption of H_2 molecules are changes in Cu–C bonds. The calculated BCP characteristics (charge densities ρ_{BCP}, Laplacians $\Delta\rho_{BCP}$ and ellipticities ε_{BCP}) and DIs of Cu–C bonds in all studied systems are given in Table S3 in ESI. In general, the differences in BCP parameters and DIs of Cu–C bonds are less than 10% in the case of Cu-dopCC + n H_2 systems or less than 15% in the case of Cu-decCC + n H_2, see Table S3. The larger differences in Cu-decCC + n H_2 system when compared to Cu-decCC + n H_2 one are due to the larger number of adsorbed hydrogens (five vs. three, respectively). Herein, we show only the dependence of

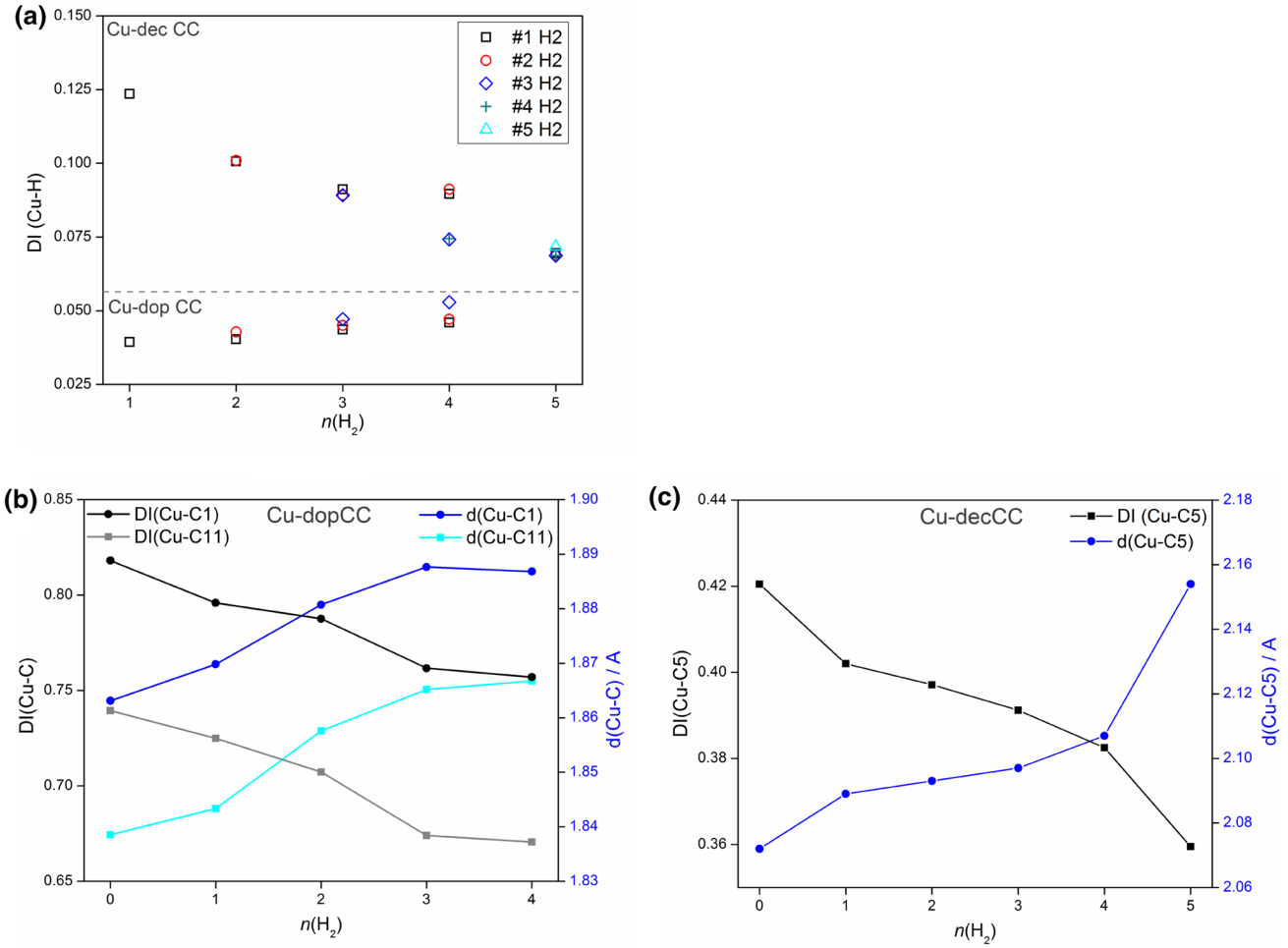

Fig. 7 **a** B3LYP-GD3/6-311G* delocalization indexes (DI) of Cu–H bonds as a function of number of adsorbed H_2 molecules [n (H_2)], **b**, **c** B3LYP-GD3/6-311G* delocalization indexes (DI) and bond distances (d) of the selected Cu–C bonds of Cu-dopCC and Cu-decCC as a function of number of adsorbed H_2 molecules [n (H_2)]

Cu–C bond lengths and corresponding DIs with respect to the number of adsorbed H_2 molecules [n (H_2)]. These dependences are presented in Fig. 7. (For the sake of simplicity the Cu–C2 bond is omitted in the case of Cu-dopCC system and only Cu–C1 and Cu–C11 are shown. Note that, trends in bond lengths and DIs of Cu–C2 bond are very similar to the ones of Cu–C1 or Cu–C11.) The increase of Cu–C distances (represented by blue and cyan lines) corresponds well with the decrease of Cu–C DI values (black and grey lines) with respect to the growing number of adsorbed H_2 molecules, see Fig. 7. Both of these trends reflect the small weakening of the Cu–C bond upon the H_2 adsorption. Note that, the H–H bonds in all adsorbed H_2 molecules are only slightly weaker (having the DI values of ca. 0.95) when compared to the H–H bond in the molecular hydrogen (DI value of 1.00).

In the case of the calculations taking the diffuse functions into account, the DI value for the Cu–H becomes considerably larger (0.305) in the case of the Cu-dopCC system, which clearly indicates chemisorption. On the contrary, the DI is smaller for the Cu-decCC system (0.077), because of the larger Cu–H distance, for the 6–311++G** basis set. This actually appears to be a considerable issue not only for the current study but also for other Cu–H interaction studies which employed the DFT/6-311G* protocol [67]

4 Conclusion

In the presented work we have theoretically studied the affinity of Cu-doped and Cu-decorated circumcoronene towards hydrogen molecules to investigate their potential use as H_2 storage materials. The obtained results point out that the adsorption ability of Cu-dopCC is limited to three H_2 molecules on one Cu atom, what is in agreement with previously reported results [29–31, 34]. On the other hand, the Cu-decCC is able to bind up to five H_2 molecules on one Cu atom. The energetic outcome of such adsorption is

within the range of −0.3 to −30 kJ mol^{-1} with respect to the number of adsorbed hydrogens (see Table 2). In general, the Cu-decCC is found to be more suitable H_2 storage material when compared to the Cu-dopCC, mainly because the Cu in Cu-decCC is sterically less hindered than the one in Cu-dopCC (see Figs. 1, 2, 3). This finding can probably be generalized also to other transition metals used as dopants or decorating atoms in graphene surfaces. However, the PDOS analysis as well as QTAIM analysis of bond critical points show that the interaction between the Cu and adsorbed H_2 molecules in the studied systems is weak and can be considered as a physisorption (see Figs. 4, 5, 6). With respect to what is mentioned above, one can conclude that the Cu-modified (doped or decorated) graphene surfaces present an alternative for currently used H_2 storage materials. However, it has to be mentioned that there are differently modified graphene surfaces, e.g. Cr-doped, [29] Fe-doped or Os-doped [30], exhibiting a better H_2 storage performance than the Cu-modified ones.

Still, it is found that the basis set choice is crucial for the systems studied, where in the case of Cu-dopCC systems the inclusion of diffuse function promises a chemisorption of the H_2 molecule at Cu, while the Cu-CC interaction becomes destabilized and the same occurs for the Cu–H_2 interaction.

Acknowledgements This work received financial support from Slovak Grant Agencies APVV (contracts No. APVV-15-0079, APVV-15-0053, APVV-19-0024 and APVV-19-0087) and VEGA (contracts No. 1/0139/20 and 1/0466/18). We are also grateful to the HPC center at the Slovak university of technology in Bratislava, which is a part of the Slovak infrastructure of high performance computing (SIVVP project, ITMS code 26230120002, funded by the European region development funds) for the computational time and resources made available. To all financing sources the authors are greatly indebted.

Compliance with ethical standards

Conflict of interest The authors declare that they have no conflict of interest.

References

1. Novoselov KS, Geim AK, Morozov SV et al (2004) Electric field effect in atomically thin carbon films. Science 306:666–669. https://doi.org/10.1126/science.1102896
2. Pykal M, Jurecka P, Karlicky F, Otyepka M (2016) Modelling of graphene functionalization. Phys Chem Chem Phys 18:6351–6372. https://doi.org/10.1039/C5CP03599F
3. Schedin F, Geim A, Morozov SV et al (2007) Detection of individual gas molecules adsorbed on graphene. Nat Mater 6:652–655. https://doi.org/10.1038/nmat1967
4. Yang W, Ratinac KR, Ringer SR et al (2010) Carbon nanomaterials in biosensors: should you use nanotubes or graphene. Angew Chemie Int Ed 49:2114–2138. https://doi.org/10.1002/anie.200903463
5. Liu Y, Dong X, Chen P (2012) Biological and chemical sensors based on graphene materials. Chem Soc Rev 41:2283–2307. https://doi.org/10.1039/c1cs15270j
6. Rodrigo D, Limaj O, Janner D et al (2015) Mid-infrared plasmonic biosensing with graphene. Science 349:165–168. https://doi.org/10.1126/science.aab2051
7. Ambrosi A, Chua CK, Bonanni A, Pumera M (2014) Electrochemistry of graphene and related materials. Chem Rev 114:7150–7188. https://doi.org/10.1021/cr500023c
8. Lv R, Terrones M (2012) Towards new graphene materials: Doped graphene sheets and nanoribbons. Mater Lett 78:209–218. https://doi.org/10.1016/j.matlet.2012.04.033
9. Zhou M, Lu Y-H, Cai Y-Q et al (2011) Adsorption of gas molecules on transition metal embedded graphene: a search for high-performance graphene-based catalysts and gas sensors. Nanotechnology 22:385502. https://doi.org/10.1088/0957-4484/22/38/385502
10. Düzenli D (2016) A comparative density functional study of hydrogen peroxide adsorption and activation on the graphene surface doped with N, B, S, Pd, Pt, Au, Ag and Cu Atoms. J Phys Chem C 120:20149–20157. https://doi.org/10.1021/acs.jpcc.6b06131
11. Wu P, Du P, Zhang H, Cai C (2013) Microscopic effects of the bonding configuration of nitrogen-doped graphene on its reactivity toward hydrogen peroxide reduction reaction. Phys Chem Chem Phys 15:6920. https://doi.org/10.1039/c3cp50900a
12. Liu S, Huang S (2017) Theoretical insights into the activation of O2 by Pt single atom and Pt4 nanocluster on functionalized graphene support: Critical role of Pt positive polarized charges. Carbon N Y 115:11–17. https://doi.org/10.1016/j.carbon.2016.12.094
13. Mohammadi-Manesh E, Vaezzadeh M, Saeidi M (2015a) Cu- and CuO-decorated graphene as a nanosensor for H2S detection at room temperature. Surf Sci 636:36–41. https://doi.org/10.1016/j.susc.2015.02.002
14. Mohammadi-Manesh E, Vaezzadeh M, Saeidi M (2015b) Theoretical study on electronic structure and electrical conductance at room temperature of Cu2O-GS nanosensors and detection of H2S gas. Comput Mater Sci 97:181–185. https://doi.org/10.1016/j.commatsci.2014.10.043
15. Maaghoul Z, Fazileh F, Kakemam J (2015) A DFT study of formaldehyde adsorption on functionalized graphene nanoribbons. Phys E Low Dimens Syst Nanostructures 66:176–180. https://doi.org/10.1016/j.physe.2014.08.015
16. Rad AS (2015) First principles study of Al-doped graphene as nanostructure adsorbent for NO 2 and N 2 O : DFT calculations. Appl Surf Sci j 357:1217–1224
17. Wanno B, Tabtimsai C (2014) A DFT investigation of CO adsorption on VIIIB transition metal-doped graphene sheets. Superlattices Microstruct 67:110–117. https://doi.org/10.1016/j.spmi.2013.12.025
18. Dai J, Yuan J, Giannozzi P (2009) Gas adsorption on graphene doped with B, N, Al and S: s theoretical study. Appl Phys Lett 95:232105. https://doi.org/10.1063/1.3272008
19. Zhou L, Shen F, Tian X et al (2013) Stable Cu2O nanocrystals grown on functionalized graphene sheets and room temperature H2S gas sensing with ultrahigh sensitivity. Nanoscale 5:1564. https://doi.org/10.1039/c2nr33164k
20. Malček M, Cordeiro MNDS (2018) A DFT and QTAIM study of the adsorption of organic molecules over the copper-doped coronene and circumcoronene. Phys E Low-Dimens Syst Nanostructures 95:59–70. https://doi.org/10.1016/j.physe.2017.09.004
21. Janani K, John Thiruvadigal D (2017) Chemical functionalization and edge doping of zigzag graphene nanoribbon with

L-(+)-leucine and group IB elements—A DFT study. Appl Surf Sci 418:406–413. https://doi.org/10.1016/j.apsusc.2017.02.192
22. Malček M, Bučinský L, Teixeira F, Cordeiro MNDS (2018) Detection of simple inorganic and organic molecules over Cu-decorated circumcoronene: a combined DFT and QTAIM study. Phys Chem Chem Phys 20:16021–16032. https://doi.org/10.1039/c8cp02035c
23. Bosch-Navarro C, Rourke JP, Wilson NR (2016) Controlled electrochemical and electroless deposition of noble metal nanoparticles on graphene. RSC Adv 6:73790–73796. https://doi.org/10.1039/C6RA14836K
24. Feng X, Lv P, Sun W et al (2017) Reduced graphene oxide-supported Cu nanoparticles for the selective oxidation of benzyl alcohol to aldehyde with molecular oxygen. Catal Commun 99:105–109. https://doi.org/10.1016/j.catcom.2017.05.013
25. Bayev VG, Fedotova JA, Kasiuk JV et al (2018) CVD graphene sheets electrochemically decorated with "core-shell" Co/CoO nanoparticles. Appl Surf Sci 440:1252–1260. https://doi.org/10.1016/j.apsusc.2018.01.245
26. Durán GM, Benavidez TE, Contento AM et al (2017) Analysis of penicillamine using Cu-modified graphene quantum dots synthesized from uric acid as single precursor. J Pharm Anal 7:324–331. https://doi.org/10.1016/j.jpha.2017.07.002
27. Lonkar SP, Deshmukh YS, Abdala AA (2015) Recent advances in chemical modifications of graphene. Nano Res 8:1039–1074. https://doi.org/10.1007/s12274-014-0622-9
28. Lin L, Zhou W, Gao R et al (2017) Low-temperature hydrogen production from water and methanol using Pt/α-MoC catalysts. Nat Publ Gr 544:80–83. https://doi.org/10.1038/nature21672
29. Xiang C, Li A, Yang S et al (2019) Enhanced hydrogen storage performance of graphene nano fl akes doped with Cr atoms : a DFT. RSC Adv 9:25690–25696. https://doi.org/10.1039/c9ra04589a
30. Tabtimsai C, Rakrai W, Wanno B (2017) Hydrogen adsorption on graphene sheets doped with group 8B transition metal : a DFT investigation. Vaccum 139:101–108. https://doi.org/10.1016/j.vacuum.2017.02.013
31. Zhou Y, Chu W, Jing F et al (2017) Applied Surface Science Enhanced hydrogen storage on Li-doped defective graphene with B substitution : a DFT study . Appl Surf Sci 410:166–176. https://doi.org/10.1016/j.apsusc.2017.03.057
32. Wang L, Chen X, Du H et al (2018) First-principles investigation on hydrogen storage performance of Li, Na and K decorated borophene. Appl Surf Sci 427:1030–1037. https://doi.org/10.1016/j.apsusc.2017.08.126
33. Yang S, Lan Z, Xu H et al (2018) A first-principles study on hydrogen sensing properties of pristine and Mo-doped graphene. Int J Nanotechnol 2018:1–5. https://doi.org/10.1155/2018/2031805
34. Faye O, Eduok U, Szpunar J et al (2017) Hydrogen storage on bare Cu atom and Cu-functionalized boron-doped graphene: a first principles study. Int J Hydrog Energy 42:4233–4243. https://doi.org/10.1016/j.ijhydene.2016.10.031
35. Faye O, Szpunar JA, Szpunar B, Chedikh A (2017) Hydrogen adsorption and storage on Palladium—functionalized graphene with NH-dopant : a first principles calculation. Appl Surf Sci 392:362–374. https://doi.org/10.1016/j.apsusc.2016.09.032
36. Ruiz ME, Garcia-Prieto J, Novaro O (1984) Theoretical studies of photoexcited state Cu atom reactions. I. excited state responsible for H2 capture. J Chem Phys 80:1529–1534. https://doi.org/10.1063/1.446902
37. Bader RFW (1990) Atoms in molecules: a quantum theory. Oxford university press, Oxford
38. Colherinhas G, Fileti EE, Chaban VV (2015a) The band gap of graphene is efficiently tuned by monovalent ions. J Phys Chem Lett 6:302–307. https://doi.org/10.1021/jz502601z
39. Colherinhas G, Fileti EE, Chaban VV (2015b) Can inorganic salts tune electronic properties. Phys Chem Chem Phys 17:17413–17420. https://doi.org/10.1039/C5CP02083B
40. Colherinhas G, Fileti EE, Chaban VV (2016) Potential energy surface of excited semiconductors: graphene quantum dot and BODIPY. Chem Phys 474:1–6. https://doi.org/10.1016/j.chemphys.2016.05.011
41. Zhu C, Yang G (2016) Insights from the adsorption of halide ions on graphene materials. Chem Phys Chem 17:2482–2488. https://doi.org/10.1002/cphc.201600271
42. Becke AD (1988) Density-functional exchange-energy approximation with correct asymptotic behavior. Phys Rev A 38:3098–3100
43. Lee C, Yang W, Parr RG (1988) Development of the colic-salvetti correlation-energy formula into a functional of the electron D. Phys Rev B 37:785–789
44. Becke AD (1993) Density-functional thermochemistry. III. The role of exact exchange. J Chem Phys 98:5648–5652. https://doi.org/10.1063/1.464913
45. Vosko SH, Wilk L, Nusair M (1980) Accurate spin-dependent electron liquid correlation energies for local spin density calculations: a critical analysis. Can J Phys 58:1200–1211. https://doi.org/10.1139/p80-159
46. Grimme S (2006) Semiempirical GGA-type density functional constructed with a long-range dispersion correction. J Comput Chem 27:1787–1799. https://doi.org/10.1002/jcc
47. Krishnan R, Binkley JS, Seeger R, Pople JA (1980) Self-consistent molecular orbital methods. XX. a basis set for correlated wave functions. J Chem Phys 72:650–654
48. McLean AD, Chandler GS (1980) Contracted Gaussian basis sets for molecular calculations. I. second row atoms, Z=11–18. J Chem Phys 72:5639–5648
49. Wachters AJH (1970) Gaussian basis set for molecular wavefunctions containing third-row atoms. J Chem Phys 52:1033–1036
50. Sousa SF, Fernandes PA, Ramos MJ (2007) General performance of density functionals. J Phys Chem A 111:10439–10452. https://doi.org/10.1021/jp0734474
51. Ramalho JPP, Gomes JRB, Illas F (2013) Accounting for van der Waals interactions between adsorbates and surfaces in density functional theory based calculations: selected examples. RSC Adv 3:13085–13100. https://doi.org/10.1039/c3ra40713f
52. Grimme S, Hansen A, Brandenburg JG, Bannwarth C (2016) Dispersion-corrected mean-field electronic structure methods. Chem Rev 116:5105–5154. https://doi.org/10.1021/acs.chemrev.5b00533
53. Mollenhauer D, Brieger C, Voloshina E, Paulus B (2015) Performance of dispersion-corrected DFT for the weak interaction between aromatic molecules and extended carbon-based systems. J Phys Chem C 119:1898–1904. https://doi.org/10.1021/jp5113312
54. Le D, Kara A, Schroder E et al (2012) Physisorption of nucleobases on graphene: a comparative van der Waals study. J Phys Condens Matter 24:424210. https://doi.org/10.1088/0953-8984/24/42/424210
55. Frisch MJ, Trucks GW, Schlegel HB, et al. (2009) Gaussian 09, Revision D.01
56. Keith TA AIMAll, version 14.04.17; TK Gristmill software: Overland Park, KS, 2014 (aim.tkgristmill.com)
57. O'Boyle NM, Tenderholt AL, Langner KM (2008) cclib: a library for package-independent computational chemistry algorithms. J Comput Chem 29:839–845. https://doi.org/10.1002/jcc.20823
58. Flükiger P, Lüthi HP, Sortmann S, Weber J "MOLEKEL 4.3." Swiss center for scientific computing: Manno, Switzerland 2002
59. Clark T, Chandrasekhar J, Spitznagel GW, Schleyer PVR (1983) Efficient diffuse function—augmented basis sets for anion calculations. III.* The 3–21 + G basis set for first-row. J Comp Chem 4:294–301. https://doi.org/10.1002/jcc.540040303

60. Boys SF, Bernardi F (1970) The calculation of small molecular interactions by the differences of separate total energies. Some procedures with reduced errors. Mol Phys 19:553–566. https://doi.org/10.1080/00268977000101561
61. Bacskay GB (1952) A quadritically convergent hartree-fock (QC-SCF) method. Application to open shell orbital optimization and coupled perturbed hartree-fock calculations. Chem Phys 65:383–396. https://doi.org/10.1016/0301-0104(82)85211-7
62. Luna-Garcia H, Ramirez-Solis A, Castillo S (2002) Ab initio studies of the reactions of Cu (2 S, 2 D and 2 P) with SiH 4 and GeH 4. J Chem Phys 116:928–935. https://doi.org/10.1063/1.1427713
63. Bhagi-Damodaran A, Michael MA, Zhu Q et al (2017) Why copper is preferred over iron for oxygen activation and reduction in haem-copper oxidases. Nat Chem 9:257–263. https://doi.org/10.1038/nchem.2643
64. López CS, de Lera ÁR (2011) Bond ellipticity as a measure of electron delocalization in structure and reactivity. Curr Org Chem 15:3576–3593. https://doi.org/10.2174/138527211797636228
65. Bader RFW, Stephens ME (1975) Spatial localization of the electronic pair and number distributions in molecules. J Am Chem Soc 97:7391–7399. https://doi.org/10.1021/ja00859a001
66. Afonin AV, Vashchenko AV, Sigalov MV (2016) Estimating the energy of intramolecular hydrogen bonds from ^{1}H NMR and QTAIM calculations. Org Biomol Chem 14:11199–11211. https://doi.org/10.1039/C6OB01604A
67. Arslancan S, Herrera B, Lamsabhi AM (2020) On the nature of the interaction of copper hydride and halide with substituted ethylene and acetylene. J Mol Model 26:61. https://doi.org/10.1007/s00894-020-4320-0